
Article:
Klenk, Jan M, Fischer, Max-Philipp, Dubiel, Paulina et al. (4 more authors) (2019) Identification and characterization of cytochrome P450 1232A24 and 1232F1 from Arthrobacter sp. and their role in the metabolic pathway of papaverine. The Journal of Biochemistry. ISSN 1756-2651

https://doi.org/10.1093/jb/mvz010

The Journal of Biochemistry, Regular Paper

Identification and characterization of cytochrome P450 1232A24 and 1232F1 from *Arthrobacter* sp. and their role in the metabolic pathway of papaverine

Jan M. Klenk[1], Max-Philipp Fischer[1], Paulina Dubiel[2], Mahima Sharma[2], Benjamin Rowlinson[2], Gideon Grogan[2], Bernhard Hauer[1,*]

[1]Department of Technical Biochemistry, Institute of Biochemistry and Technical Biochemistry, University of Stuttgart, Allmandring 31, 70569 Stuttgart, Germany;

[2]Department of Chemistry, University of York, Heslington, York, YO10 5DD, United Kingdom

***Running title*:** Characterization of P450s from *Arthrobacter* sp.

*To whom correspondence should be addressed: Prof. Bernhard Hauer: Institute of Biochemistry and Technical Biochemistry, University of Stuttgart, Allmandring 31, 70569 Stuttgart, Germany; bernhard.hauer@itb.uni-stuttgart.de; Tel: +49 711 685 63193, Fax: +49 711 685 63196

Topics: Enzymology (Biochemistry), Protein structure (Biochemistry), Metabolism (Biochemistry)

Abbreviations:

CamA, Putidaredoxin reductase; CamB, Putidaredoxin; cww, cell wet weight; FeRed_1, Ferredoxin reductase; FlavRed, Flavodoxin reductase; FldX, Flavodoxin; IMAC, Immobilized metal affinity chromatography; IEX, Ion exchange chromatography; P450, Cytochrome P450 monooxygenase; 5-Ala, 5-Aminolevulinic acid; 3,4-Dimethoxyphenylacetic acid, 3,4-DMPA.

Summary

Cytochrome P450 monooxygenases (P450s) play crucial roles in the cell metabolism and provide an unsurpassed diversity of catalyzed reactions. Here, we report the identification and biochemical characterization of two P450s from *Arthrobacter* sp., a gram-positive organism known to degrade the opium alkaloid papaverine. Combining phylogenetic and genomic analysis suggested physiological roles for P450s in metabolism, and revealed potential gene clusters with redox partners facilitating the reconstitution of the P450 activities *in vitro*. CYP1232F1 catalyzes the *para* demethylation of 3,4-dimethoxyphenylacetic acid to homovanillic acid while CYP1232A24 continues demethylation to 3,4-dihydroxyphenylacetic acid. Interestingly, the latter enzyme is also able to perform both demethylation steps with preference for the *meta* position. The crystal structure of CYP1232A24, which shares only 29% identity to previous published structures of P450s helped to rationalize the preferred demethylation specificity for the *meta* position and also the broader substrate specificity profile. In addition to the detailed characterization of the two P450s using their physiological redox partners, we report the construction of a highly-active whole-cell *E. coli* biocatalyst expressing CYP1232A24, which formed up to 1.77 g l^{-1} 3,4-dihydroxyphenylacetic acid. Our results revealed the P450s' role in the metabolic pathway of papaverine enabling further investigation and application of these biocatalysts.

Keywords: *Arthrobacter* sp., biochemical characterization, crystal structure, cytochrome P450, metabolism

The gram-positive organism *Arthrobacter* sp. can be classed with the family of *Micrococcaceae* and represents the genus with the largest number of species (1). As one of the most commonly isolated soil bacteria, *Arthrobacter* sp. exhibits a remarkable adaptivity to extreme environmental conditions and metabolic diversity (2–5). In addition to the degradation of harmful aliphatic, aromatic and organic compounds, the bacterium is able to metabolize the naturally occurring complex opium alkaloid papaverine for energy supply (6–8). Possible metabolic pathways of the degradation of compounds such as papaverine, phthalates or sulfadiazines have already been postulated (6, 9–13) however, the enzymes involved are often not known or have not yet been heterologously expressed for detailed characterization.

The first step in the degradation of xenobiotics is often catalyzed by oxygenases, such as dioxygenases, or by cytochrome P450 monooxygenases (P450s). The latter enzyme system represents a huge and diverse superfamily, which can be categorized into families (> 40% identity) and subfamilies (> 55% identity). Based on the associated electron-donating redox partners, the P450s are further divided into different electron transfer classes (I to VIII) (14, 15). Their ability to oxyfunctionalize non-activated carbon-hydrogen bonds using molecular oxygen under mild reaction conditions (RT, atmospheric pressure) renders P450s highly attractive for applications in chemical synthesis (16, 17). Unfortunately, the identification of novel P450s for potential industrial applications is often quite challenging due to the complexity of the enzyme system. For this, several factors must be overcome: I) functional expression of all components, II) determination of functional redox partners, which are mainly distributed over the whole genome, III) lack of knowledge regarding the physiological function of the enzymes. Although it is often possible to reconstitute the enzymes' activity by non-physiological redox partners like eukaryotic adrenodoxin reductase and adrenodoxin from *Bos taurus* as well as putidaredoxin reductase (CamA) and putidaredoxin (CamB) from *Pseudomonas putida*, using the physical redox partners in most cases results in higher activity. However, the search for an entire functional multicomponent-substrate-system can be tedious and is a factor limiting the investigation and also the activity of P450s (18). In the last decade, interesting P450s were successfully characterized from metabolically diverse bacteria including *Bacillus megaterium*, *Chondromyces apiculatus*, *Novosphingobium aromaticivorans*, *Rhodopseudomonas palustris* and *Sorangium cellulosum* (19–23).

Nevertheless, the gap between characterized P450s and available sequences is consequently increasing due to progress in genome sequencing technology. Recently, the 4.8-Mb draft genome of *Arthrobacter* sp. isolated close to Hohenheim (DE), which was formerly known as *Nocardia* sp. was sequenced by our group and phylogenetically reclassified (24). In the late 1970s, metabolites accumulating in the medium were analyzed when this strain was cultivated on papaverine as sole carbon and nitrogen source (6, 9). Thus, a partial metabolic pathway of papaverine was proposed which consists of multiple enzymatic steps including reactions possibly catalyzed by P450s (Fig. 1). By decoding the genome, the investigation of four putative P450s, as well as many different oxygenases and redox proteins from this metabolically diverse organism was enabled. The reconstitution of P450 activity and identification of substrates oxyfunctionalized by these enzymes might provide novel insights into P450 systems while revealing new biocatalysts for potential industrial applications.

In this study, we cloned, expressed and characterized two novel P450s from *Arthrobacter* sp. which together catalyze the didemethylation of 3,4-dimethoxyphenylacetic acid (3,4-DMPA), through their complementary specificity for *meta*- and *para*-methoxy groups. In the course of these studies, we discovered a putative P450 class III system consisting of a physiological ferredoxin reductase and flavodoxin for electron transfer. The crystal structure of one of the enzymes, CYP1232A24, in combination with computer-modelling, has revealed the molecular determinants of *meta* specificity in the enzyme. Finally, efficient whole-cell recombinant biocatalysts were constructed by expressing the enzymes in *E. coli*, enlarging the biotechnological potential for selective oxyfunctionalization.

Experimental Procedures

Growth experiments with Arthrobacter sp.

The cultivation of *Arthrobacter* sp. was carried out in liquid culture with 20 ml MSB minimal medium (as described by Cohen-Bazire and Stanier (25)) containing 1% glucose at 30°C and 180 rpm overnight (Table S1). Testing alternative carbon sources, a preculture grown in glucose was centrifuged and resuspended in 200 ml MSB medium with 0.1% of the corresponding carbon source. Starting from an OD_{600} of 0.1, the optical density was measured periodically to determine growth of the organism.

Proteomic analysis

Samples cultivated on different carbon sources were harvested at OD_{600} of approx. 1.6 by centrifugation and lysed through enzymatic and mechanical methods. The cells were resuspended in 3 ml per g cell wet weight (g_{cww}) lysis buffer (20 mM Tris/HCl pH 7.5, 1 mM EDTA, 1% Triton-X, 100 mM NaCl, directly before use: 1 mM DTT, 20 µg ml^{-1} DNase I and protease inhibitors: 1 µM Pepstatin, 0.1 mM AEBSF, 0.1 mM PMSF) and treated with lysozyme for 2 h at 37°C. Subsequently, the lysis was continued through a high-pressure homogenizer (EmulsiFlex-C5, Avestin, Ottowa, Canada) for 5 x 5 min cycles under 1700 bar pressure. Remaining DNA was sheared by sonification on ice (Branson Sonifier 250 equipped with a microtip: 3 mm diameter, Danbury, USA) for 5 min (pulse: Output 5 – 6, Duty cycle: 35%). To obtain detailed information of the proteins location the lysed cells were centrifuged for 30 min at 55,000 x g and 4°C (Beckman Avanti J-26S XP with a JA-25.50 Rotor, Beckman Coulter, Brea, California, USA) to obtain the soluble (cell lysate) and insoluble (cell debris) fraction. The proteome of the samples was visualized through 10% and 12% SDS-PAGE. The following proteomic analysis was conducted by the mass spectrometry unit at the University of Hohenheim (DE). In this respect, the proteins were isolated from the SDS-PAGE, trypsin digested and the resulting peptide fragments analyzed using an ACQUITY nano-UPLC system (Waters GmbH, Milford, USA) directly coupled to a LTQ-Orbitrap XL hybrid mass spectrometer (Thermo Fisher Scientific, Bremen, Germany) as described elsewhere (26). The detected peptides were compared with a list of endogenous oxidation/reduction proteins derived by the genome of *Arthrobacter* sp. as well as with the global NCBI database using the MASCOT search algorithm to identify the corresponding proteins. The mass spectrometry proteomics data have been deposited to the ProteomeXchange Consortium *via* the PRIDE (27) partner repository with the dataset identifier PXD009566 and 10.6019/PXD009566.

Genomic analysis

LGC Genomics® (Berlin, Germany) performed the global annotation of the draft genome of *Arthrobacter* sp. (24) Using this information, the corresponding ORFs of oxidation/reduction proteins were visualized in the software snapgene and investigated by comparison with the global NCBI

database. Finally, Prof. David Nelson (Health Science Center, University of Tennessee) thankfully assigned the P450 families and subfamilies based on the common nomenclature.

Cloning

The genomic DNA of *Arthrobacter* sp. was isolated from a preculture grown with 1% glucose using the Gene JET Genomic DNA Purification Kit (Thermo Fisher Scientific, Waltham, USA). The genes of CYP1232A24 (WP_091470958), CYP1232F1 (WP_091470959), FldX (WP_091470964), FeRed_1 (WP_091470967) and FlavRed (WP_091470969) were amplified by PCR using the *PfuUltra* II fusion HS DNA polymerase. Appropriate primers were designed to introduce *Nde*I as well as *Eco*RI or *Hind*III restriction sites on the 3'-fragment ends. Thereby, from *E. coli* more frequently used start and stop codons were introduced as required. After PCR amplification, the fragments were subsequently subcloned into the pET-28a(+) vector behind the poly-histidine-tag through the corresponding restriction sites. In case of low expression levels of the protein the gene was subcloned into pCWori^{+} or pBAD33 using the *Nde*I and *Hind*III restriction sites or Gibson Assembly®. DNA sequencing (GATC Biotech AG, Konstanz, Germany) verified the correct constructs. The sequences of the primers and the PCR procedure are given in Table S2 and S3.

Expression and purification of P450s and redox partners

The heterologous protein expression in *E. coli* was carried out as described previously (20) and induced as listed in supplementary Table S4 to start protein expression. Cells containing a protein with a poly-histidine-tag (FldX, FeRed_1, FlavRed, CamA, CamB) were purified by immobilized metal affinity chromatography as described elsewhere (20). CYP1232F1 and CYP1232A24 were purified *via* anion exchange chromatography using a Toyopearl DEAE 650M XK16/40 30 ml cv column and a GigaCap DEAE 650M XK50/20 90 ml cv column (both Tosoh Bioscience, Griesheim, Germany), respectively, applying the respective buffers and conditions as described previously (20). The IMAC and IEX purified proteins were concentrated as well as the buffer exchanged through Vivaspin20 columns (cutoff 10 kDa, Sartorius, Goettingen, Germany) to 50 mM KPi pH 7.0 (150 mM NaCl, 10 % Glycerol). Finally the proteins were aliquoted to 200 µL and stored at -20°C until use.

Determination of protein concentration

The P450 concentrations were determined by CO-difference spectroscopy according to the method of Omura and Sato using $\varepsilon_{450\text{-}490} = 91$ mM^{-1} cm^{-1} (28). The extinction coefficient of the *Arthrobacter* sp. reductase FeRed_1 was determined at 454 nm ($\varepsilon_{454} = 10.69$ mM^{-1} cm^{-1}) by quantification of the flavin content using CamA as positive control as described by Bell and co-workers (29). Novel putative flavodoxin FldX not showing any distinct absorption maximum in the range of 300 - 600 nm did not allow for specific concentration measurement. Therefore, BCA Protein Assay of the purified FldX solution was performed according to manufacturer's instructions resulting in a protein content of 29 ± 0.3 mg ml^{-1}. In case of the literature known redox partners following extinction coefficients were used for quantification:

- CamA: average of 378, 454 and 480 nm; (ε) 9.7, 10.0 and 8.5 mM^{-1} cm^{-1} (30)
- CamB: average of 415 and 455 nm; (ε) 11.1 und 10.4 mM^{-1} cm^{-1} (30)

Purities of the purified proteins were controlled by SDS-PAGE.

Purification and Crystallization of CYP1232A24

The gene encoding CYP1232A24 was subcloned into the pETYSBLIC-3C vector using protocols described previously (31). The recombinant plasmid was used to transform *E. coli* Arctic Express cells. A single colony of the recombinant strain was used to inoculate 10 ml of culture of TB medium containing 30 µg ml^{-1} of kanamycin. This overnight culture was used for inoculation of 500 ml of the same medium and the cultivation was continued at 37°C shaking until a OD_{600} reached a value of 1.0. Then, the culture was induced with 0.4 mM IPTG and the medium supplemented with 0.4 mM $FeSO_4$ and 0.4 mM 5-Aminolevulinic acid (5-Ala). The culture was incubated overnight at 18°C with shaking. Cells were harvested by centrifugation for 30 min at 5,000 x g. The pellets were then resuspended in a buffer containing 50 mM K_2PO_4, 300 mM KCl, protease inhibitor (0.1 mM PMSF) and 30 mM imidazole at pH 7.5. The cells were disrupted using ultrasonication and the resulting suspension centrifuged for 45 min at 50,000 x g at 4°C. The soluble fraction was loaded onto a nickel column that had been pre-equilibrated with the buffer and eluted with an increasing gradient of imidazole to a concentration of 500 mM. Fractions containing the protein of interest were pooled together,

concentrated to a volume of 500 µl and loaded onto a size exclusion column (S200) that had been pre-equilibrated with a buffer containing 50 mM Tris and 300 mM NaCl at pH 7.5. Protein-containing fractions were analysed on a 12% SDS-PAGE gel and the appropriate fractions were pooled together and concentrated using vivaspin20 columns (cutoff 10 kDa) for crystallization trials. Purity of the P450 was estimated to be greater than 95% by SDS–PAGE analysis (Fig. S1) and the protein concentration determined by CO-difference spectroscopy as described above.

CYP1232A24 was subjected to crystallization trials using the purified protein at a concentration of 15 mg ml^{-1} using the sitting drop vapour diffusion method in which a Mosquito robot was used to dispense drops of 150 nl of protein solution and 150 nl of the precipitant from a range of commercial screens. Crystals grew in conditions containing 0.1 M Bis-Tris propane buffer at pH 6.5, with 20% (w/v) polyethylene glycol monomethyl ether 5000. Crystals were harvested from these drops into a cryoprotectant solution containing 15% ethylene glycol in the mother liquor and were flash-cooled in liquid nitrogen for diffraction tests.

Data collection and refinement

A complete dataset for CYP1232A24 was collected at the Diamond Light Source (Didcot, Oxfordshire, United Kingdom) on beamline I04-1. The data were processed and integrated using XDS (32) and scaled using SCALA (33) as part of the Xia2 processing system (34). Data collection statistics are given in Table 1. Crystals of CYP1232A24 were in space group $P2_1$. The structure was solved applying MOLREP (35), using the cytochrome P450 PikC 2VZ7 (36) as the search model. The crystal contained one monomer in the asymmetric unit and the solvent content was 47.6%. The structure was built and refined using iterative cycles using Coot (37) and REFMAC (38) (Fig. S2). The final structure had R_{cryst} and R_{free} values of 20.8% and 22.9%. Refinement statistics are presented in Table 1**.** The Ramachandran plot showed 95.6% of residues in allowed regions and 4.4 in preferred regions, with no outliers. The coordinate files and structure factors have been deposited in the Protein DataBank (PDB) with the coordinate accession number **6G71**.

Bioinformatics tools

Molecular docking of 3,4-DMPA into the P450 active pocket was performed using the AutoDock Vina algorithm implemented in YASARA. The water molecules inside the active site and the channel were retained for the docking experiment.

Substrate binding – Spin-state measurements

To determine the spin-state shifts of the novel P450s upon substrate-binding, the induced spin-shifts were assayed at 30°C using microtiter-plates and a plate reader (PolarStar Omega 96 well, BMG Labtech GmbH, Ortenberg, Germany). 1 µl of substrate (1, 5 or 50 mM stock solution in DMSO) was stepwise added to 200 µl of a 3 µM P450 solution in IMAC buffer and spectra between 320 – 480 nm recorded each time. The measurements were performed in triplicates while 3 µM P450 solution with the same volume of pure DMSO was used as reference to compensate dilution effects. A shift in absorbance (ΔA) was determined by subtracting the sample with substrate from the reference. Finally, for the determination of the binding constants K_d, the difference ΔA_{390} - ΔA_{420} was plotted against the substrate concentration used and a hyperbolic curve was fitted applying the solver analysis tool in Excel (Eqn. 1):

$$\Delta A = \frac{\Delta A_{max} * [S]}{K_d + [S]}$$

ΔA is the peak-to-trough absorbance difference, ΔA_{max} is the maximum absorbance difference and [S] is the substrate concentration.

In vitro assays

The *in vitro* reactions were carried out in a volume of 200 µl in reaction buffer (50 mM KPi pH 7.0, 150 mM NaCl, 2.5% glycerol). The glucose-6-phosphate dehydrogenase system (G6PDH from *L. mesenteroides*) was used to regenerate the cofactor NAD(P)H (12 U ml^{-1} G6PDH, 5 mM G6P, 1 mM $MgCl_2$). Standard *in vitro* reactions contained 100 µg ml^{-1} catalase, 2 mM NAD(P)H and 1 mM substrate (50 mM stock solution in DMSO or ethanol). All components were mixed, and the biotransformation was started with the addition of a mixture of P450 (lysate or purified), reductase, flavodoxin or ferredoxin in the stoichiometric ratio 1: 1.5: 15 (2 µM: 3 µM: 30 µM). In the case of the

FeRed_1 and FldX redox partner system, 225 µM from purified FldX solution was used. The reactions were incubated for 0.5 – 24 h at 30°C and 180 rpm, stopped by 10 µl 37% HCl or directly by organic solvent and then prepared for gas chromatography. Negative controls were either lysates generated by the expression of the empty vector, or in the case of reactions with purified P450s, all reaction components except the P450. Examples of investigated substrates are listed in Table S5.

NAD(P)H depletion assay and determination of coupling efficiencies

For the NAD(P)H assay, purified P450s and redox partners were used in reaction buffer employing a stoichiometric ratio of 1: 1.5: 15, respectively. In total 0.25 µM P450 was deployed in reaction buffer with a final volume of 200 µl in microtiter plates. In the case of the redox partner combination FeRed_1 and FldX, 60 µM from purified FldX solution was used. The components were mixed together with 100 µg ml^{-1} catalase and 0.5 mM substrate (5 mM stock solution in DMSO). After 2 min of incubation at 30°C, the reaction was started with 300 µM NAD(P)H (5 mM stock solution in reaction buffer) and the decrease of NAD(P)H monitored at a wavelength of 340 nm on the plate reader as described elsewhere (46). After the cofactor was completely consumed, the reactions were stopped by 10 µl 37% HCl and the product formation was later quantified through gas chromatography. The reactions were carried out in triplicates while reactions without substrate addition served as a reference. A new calibration of NAD(P)H was measured for each 96-well plate to quantify the cofactor depletion. To determine coupling efficiencies, the product formation was finally correlated to the cofactor depletion while the values of the reference were subtracted to correct the background caused by protein impurities (Fig. S3).

Determination of kinetic constants

To fulfill steady-state kinetics, different enzyme concentration ratios and reaction times were tested, so that a maximum conversion of 10% was achieved at the lowest substrate concentration. The reactions were carried out in a total volume of 500 µl in 50 mM KPi pH 7.0 and contained a non-limiting concentration of the cofactor NAD(P)H of 2 mM as well as 100 µg ml^{-1} catalase. The latter should exclude the denaturation of the proteins by possibly formed hydrogen peroxide through uncoupling reactions. P450, CamA and CamB were used in a ratio of 1: 1.5: 15, whereas the system P450, FeRed_1

and FldX was used at 1: 1.5: 112.5. The substrate concentrations (1 – 1000 µM) were adjusted by different stock solutions in DMSO, so that a DMSO concentration of 2% v/v was present in each reaction. First, buffer, cofactor, catalase, and substrate were mixed in 1.5 ml reaction vessels and incubated for 5 min at 30°C. To start the reactions, 100 µl of a short-preheated enzyme mixture containing the P450 and redox partners were added *via* a multistepper and the reaction was carried out in a thermocycler at 30°C and 750 rpm. The following setups were used for the recorded kinetics prepared in triplicates:

- 0.04 µM CYP1232F1 + CamA, CamB, 3,4-DMPA: 30 min
- 0.03 µM CYP1232F1 + FeRed_1, FldX, 3,4-DMPA: 20 min
- 0.03 µM CYP1232A24 + FeRed_1, FldX, homovanillic acid: 20 min

To stop the reaction, 50 µl of 50% water/HCl solution was added and mixed by vortexing. Finally, the product formation was quantified by gas chromatography. Hereby obtained Michaelis-Menten kinetics were fitted by the Excel solver tool to determine the enzyme specific constants K_m and k_{cat}.

Construction and expression of whole-cell systems

Dual vector systems were created based on the compatible pETDuet and pCola or pBAD18 and pBAD33 vectors. The plasmids pCola_CYP1232F1_FldX, pETDuet_FldX_FeRed_1, pCola_CYP1232F1_CamB, pBAD18_FldX_FeRed_1 were constructed *via* Gibson Assembly® using the specific primers listed in Table S2. The fragments (vectors and inserts) amplified through PCR (Table S3) were controlled by an agarose gel and isolated using the Zymoclean™ Gel DNA Recovery Kit (Zymo Research Corp., Irvine, California, USA) for purification. Gibson Assembly® was finally performed with 15 µl Gibson Assembly® mix and 5 µl DNA mix (vector to insert(s), molar ratio 1:5, total ~ 300 ng) for 1 h at 50°C. After transformation in chemically competent *E. coli* XL1-blue cells, isolated plasmid constructs were checked for correct modification by DNA sequencing. For the whole-cell expression, the plasmids encoding the redox partners were transformed in competent *E. coli* BL21 (DE3) or JW5510 cells to prepare chemical competent cells of these strains. As next step, the second plasmid encoding the P450 gene was freshly transformed with high transformation efficiency

each time. Expression of the three proteins was conducted as described with the sole components using expression temperature and inductor concentration as listed in supplementary Table S4. After expression of the dual-vector systems, the cells were harvested for 15 min at 6,000 x g and 4°C and the resulting pellets directly resuspended with 100 mM KPi pH 7.0 supplemented with 30 mM glucose (to 0.2 g_{cww} ml^{-1}).

In vivo biotransformations

The resting cell reactions were finally performed in screwable 20 ml glass reaction vessels with a reaction volume of 1 ml, a final cell concentration of 0.1 g_{cww} ml^{-1}, with 30 mM glucose and with 5 or 10 mM substrate (250 mM or 500 mM stock solution in DMSO) for 24 h at 30°C and 180 rpm. The reactions were then transferred to 2 ml reaction vessels, centrifuged and the supernatant prepared for gas chromatography.

Product analysis

Highly volatile molecules or molecules whose volatility can be increased by derivatization have been analyzed by gas chromatography. For this purpose, the *in vitro* (200 µl) or *in vivo* (supernatant: 750 µl) samples were extracted with the same volume methyl tert-butyl ether (MTBE) containing 0.2 mM carvone as internal standard. In the case of a necessary derivatization of the analytes, acidification of the samples by 10 µl (*in vitro*) or 35 µl 37% HCl (*in vivo*) was performed before these were extracted with MTBE (including 0.3 mM 3-methoxyphenylacetic acid or 4-methoxycinnamic acid as internal standard). Before derivatization, the organic phase was evaporated on a Genevac EZ-2 Plus Evaporator (SP Scientific, Ipswich, United Kingdom) to dryness and the residual dissolved in a mixture of 50% MTBE and 50% N,O-bis(trimethylsilyl)trifluoroacetamide (BSTFA) + trimethylchlorosilane (TMCS) (99: 1). The derivatization of the samples (*in vitro* or kinetics: 90 µl, *in vivo*: 300 µl) was carried out in GC vials for 30 min at 70°C. If product standards were available, a calibration with the authentic standard was treated and analyzed similar to the reactions (Table S5). Gas chromatography was performed on a Shimadzu GC-2010 equipped with an AOC-20i autoinjector (Shimadzu, Nakagyo-ku, Japan). The samples were injected with different split ratios (injector temperature 250°C, carrier gas

H_2, 30 cm sec^{-1}) and separated *via* a DB-5 or HP-1ms-ui column (both 30 m x 0.25 mm x 0.25 µm, Agilent Technologies Inc., Santa Clara, California, USA). The analytes were detected by means of a flame ionization detector (FID, detector temperature 330°C) using the programs listed in Table S6.

For initial product identification, the samples were afterwards analyzed on a Shimadzu GCMS-QP2010 detector equipped with an AOC-5000 autoinjector (Shimadzu) and helium as carrier gas (linear velocity 30 cm sec^{-1}). The analytes were separated *via* a DB-5 column and measured with identical temperature programs to the previous analysis. An ionization (EI, electron ionization) of 70 eV, an interface temperature of 250°C and an ion source temperature of 200°C were used for recording the mass spectra. The mass fragments were finally detected in the scan mode from 35 to 300 *m/z* or from 40 to 450 *m/z* for the derivatized samples. The non-volatile compounds diclofenac and papaverine were analyzed by HPLC (Table S7).

Results

Proteomic and genomic analysis of Arthrobacter sp.

In previous work in our group, shotgun genome sequencing of *Arthrobacter* sp. revealed potential new P450 monooxygenases and many other oxidoreductases with putative hydroxylation activity (24). A targeted approach to identify enzymes involved in the degradation of certain molecules is proteomic analysis. In the case of growth on certain substances, enzymes like P450s, which are responsible for the observed organism's capabilities, might be overexpressed or initially induced. *Arthrobacter* sp. is able to metabolize the naturally occurring alkaloid papaverine for energy supply (6). Due to its complexity, papaverine is an interesting compound for which the key metabolic enzymes have not yet been identified and characterized. In addition to papaverine, *Arthrobacter* sp. metabolized valuable sesquiterpenes like β-bisabolene as sole carbon source. Analyzing the difference in the proteome of the gram-positive organism grown on different substrates, cell samples were lysed through a mixture of mechanical and enzymatic methods. Subsequent SDS-PAGEs already indicated variations in the protein bands depending on the substrate (Fig. S4). Compared to the control grown on glucose, CYP1232A24 and F1 could be clearly identified in the proteomic analysis of the papaverine samples while no greater difference was observed with the other substrates (Table 2). Frequently, P450 enzymes and their

electron transfer partners are widely scattered on the genome. Interestingly, the genes coding for both these P450s are located directly successively on the genome of *Arthrobacter* sp. and are associated with a possible gene cluster. This cluster consists of a ferredoxin reductase FeRed_1, which was also exclusively detected in the papaverine sample, a second reductase FlavRed and a putative flavodoxin FldX (Fig. 2). In addition, *Arthrobacter* sp. contains a large range of potential P450 redox partners like bifunctional reductases (POR and PDR homologues), 2Fe-2S or 4Fe-4S ferredoxins and several reductases which are known from biological diversity (39).

Cloning, expression and activity reconstitution of Arthrobacter sp. P450s

The genes encoding the P450s and their possible physiological redox partners were amplified from the genomic DNA and cloned into pET-28a(+). Due to the high GC content of the gene sequences and the numerous rare codons, it was found that expression of the *Arthrobacter* sp. proteins was conducted most efficiently in *E. coli* Rosetta (DE3). Nevertheless CYP1232A24 and F1 could not be expressed in satisfactory amounts even after extensive experiments with further expression strains, different media and expression temperatures and were therefore subcloned into the vectors pCWori^{+} and pBAD33. This resulted in a huge increase in potentially active P450 enzyme enabling successful purification by anion exchange chromatography (Table S4 and S8). Both purified P450s could be detected according to the calculated molecular weight on a control SDS-PAGE (Fig. 3). In case of the potential redox partners, soluble target proteins were obtained by expression from pET-28a(+) in *E. coli* Rosetta (DE3). Only FeRed_1 showed unique absorption maxima in the UV spectrum at 373 and 454 nm (Fig. S5). The extinction coefficient at 454 nm was determined as 10.69 mM^{-1} cm^{-1} and subsequently used for concentration measurements.

The identification of the right combination of enzyme, appropriate redox partners and substrate poses a challenge for the initial characterization of P450s. Both novel P450s could be assigned to the CYP1232 family of which, so far, no family members have been characterized (Table S9). The results from the proteomic analysis, however, provided strong indications for potential substrates for the initial reconstitution of activity. Fragments of CYP1232A24 and CYP1232F1 were only detected in the culture grown on papaverine as the sole carbon source. Since the P450s emerge in potential clusters with their

putative redox partners, we tested the reconstitution by these physiological redox partners FlavRed, FeRed_1 and FldX. Studies of the degradation products of papaverine have been carried out many years ago and revealed three possible P450-catalyzed reactions, such as the dihydroxylation of papaverine and twofold demethylation of 3,4-dimethoxyphenylacetic acid (3,4-DMPA) (Fig. 1) (6, 9). Notably, both enzymes showed a high demethylation activity with FeRed_1 and FldX using NADPH as a cofactor. While 2 μM CYP1232F1 converted the entire 2 mM 3,4-DMPA at the *para* position to homovanillic acid, a complete twofold demethylation to 3,4-DMPA occurred using 2 μM CYP1232A24. In contrast, hydroxylation or demethylation of papaverine was not observed in biotransformations using both P450s. In addition, we investigated a possible electron transfer by the non-physiological redox partners CamA and CamB from *P. putida* for activity reconstitution. Interestingly, 2 mM 3,4-DMPA was converted > 99% by 2 μM CYP1232F1 in combination with 3 μM CamA and 30 μM CamB, while CYP1232A24 showed only minimal activity.

Substrate specificity profiles of CYP1232A24 and CYP1232F1

The reconstitution of a functional combination of P450, redox partners and the appropriate substrate allowed for further characterization. Determining the potential of the novel biocatalysts, we investigated foremost the substrate specificity profile. Hereby, CYP1232F1 was reconstituted with CamA and CamB while CYP1232A24 was used with FeRed_1 and FldX, respectively.

In particular, *para*- and *meta*-substituted benzoic, phenylacetic, and cinnamic acid derivatives were tested (Table S5). In addition, structurally similar compounds were selected to investigate the influence of the acid group and the aromaticity. Since *Arthrobacter* sp. was able to grow on terpenes, we also screened compounds like β-bisabolene and β-ionone. CYP1232F1 displayed a very narrow substrate specificity profile (Fig. 4). 3,4-DMPA turned out to be the by far best tested substrate, as it was demethylated selectively in the *para* position to homovanillic acid completely. Among the many *para*- and / or *meta*-substituted carboxylic acids or aromatics, isohomovanillic acid, eugenol, 3-chloro-4-methoxyaniline and 3-methoxyphenylacetic acid were demethylated by CYP1232F1. The activity was reduced clearly in case of the demethylation in *meta* position, as well as when the *meta* substituent was a hydroxy group.

For CYP1232A24 a rather broad substrate specificity profile could be identified. In addition to differently substituted phenylacetic acid derivatives, the catalyst also accepted benzoic acids, such as isovanillic acid or 4-methoxycinnamic acid (Fig. 5). In contrast to CYP1232F1, CYP1232A24 demethylated *meta*- and *para*-substituted aromatic compounds such as 3-methoxyphenylacetic acid or isohomovanillic acid with high activities. Furthermore, lauric acid was hydroxylated to a small extent in the ω^{-1}-, ω^{-2}- and ω^{-3}-positions. Interestingly, hydroxylation of the terpene β-ionone in the allylic position to 4-hydroxy-β-ionone, and a demethylation of naproxen could be achieved. However, the highest activity was observed for homovanillic acid.

Biochemical characterization of CYP1232A24 and CYP1232F1

The *in vitro* biotransformations provided first indications of potential physiological substrates. In this respect, we determined the substrate binding by spin-state measurements to confirm the results obtained so far. In case of CYP1232F1, 3,4-DMPA led to a high-spin shift with the dissociation constant K_d = 65.1 ± 1.2 μM (Fig. 6), while isohomovanillic acid showed only a slight shift to a wavelength of 390 nm. No shift was observed for homovanillic acid as substrate. In contrast, the spin-state experiments with CYP1232A24 resulted in lowest dissociation constant and hence, strongest binding of homovanillic acid (K_d = 22.3 ± 0.4 μM) (Fig. 6). The binding affinity decreased with isohomovanillic acid (K_d = 80.1 ± 2.1 μM) over 3,4-DMPA where only minor high-spin shifts and no maximum were reached in the spin-state measurements using 1250 μM substrate (Fig. S6). Papaverine as substrate did not induce spin-state shifts in both enzymes.

Using the best identified substrates, we further investigated the efficiency of electron transfer and kinetic properties of the novel *Arthrobacter* sp. P450s. CYP1232A24 in combination with FeRed_1 and FldX showed an NADPH oxidation rate of 87.8 ± 2.8 nmol $nmol_{P450}^{-1}$ min^{-1} with the substrate homovanillic acid (Table S10, Fig. S3). Herein, a high coupling efficiency of 87.0 ± 0.8% was obtained. *In vitro* biotransformations using these redox partners and 2 mM homovanillic acid as substrate led to > 99% demethylation to 3,4-dihydroxyphenylacetic acid after 30 min (Table 3). In case of CYP1232F1, 2 mM 3,4-DMPA was selectively demethylated to yield > 99% of homovanillic acid in combination with FeRed_1 and FldX after 30 min. Thereby, higher NADPH oxidation rates of

103.8 ± 4.6 nmol $nmol_{P450}^{-1}$ min^{-1} could be achieved with > 99% coupling efficiency. The CYP1232F1 system was also used to check the cofactor specificity of FeRed_1. In contrast, only low oxidation rates and coupling efficiencies could be measured using NADH as cofactor. In addition, the commonly applied CamA and CamB from *P. putida* were also tested as alternative redox partners to supply electrons to CYP1232F1, which achieved NADH oxidation rates of 28.2 ± 0.4 nmol $nmol_{P450}^{-1}$ min^{-1}, a coupling efficiency of 83.7 ± 1.0% and an *in vitro* product formation of 88.1 ± 2.8% after 30 min.

The conversion of homovanillic acid to 3,4-dihydroxyphenylacetic acid by CYP1232A24 proceeded at a catalytic rate k_{cat} = 5.23 ± 0.28 min^{-1} with FeRed_1 and FldX and demonstrated K_m = 6.69 ± 0.27 µM (Table 3 and Fig. 7). The reaction properties of the demethylation of 3,4-DMPA to homovanillic acid by CYP1232F1 were investigated with the heterologous redox partners CamA and CamB and the physiological redox partners FeRed_1 and FldX from *Arthrobacter* sp, respectively. With FeRed_1 and FldX, k_{cat} was determined to be 5.40 ± 0.03 min^{-1} compared to 2.28 ± 0.04 min^{-1} with CamA and CamB. The K_m values depended on the P450 domain as well as the substrate and were therefore nearly identical with 5.16 ± 0.17 and 5.18 ± 0.20 µM. In total, the highest rates were achieved with the physiological redox partners. The catalytic efficiency values (k_{cat} K_m^{-1}) reached 7.82 * 10^5 and 1.05 * 10^6 min^{-1} M^{-1} with FeRed_1 and FldX as electron transfer partners for CYP1232A24 and CYP1232F1, respectively.

Structure of CYP1232A24

The structure of CYP1232A24 was determined to a resolution of 1.7 Å. The sequence of CYP1232A24 displays only 29% sequence identity to the closest homolog in the PDB, the P450 PikC from *Streptomyces venezuelae* (2VZ7) (36) which was used as the model in the molecular replacement solution of the structure. The crystal was in the $P2_1$ space group and featured one molecule in the asymmetric unit. The sequence was complete in the structure save for two short sequences from positions 68-69 and 216-218 for which the electron density was insufficient for modelling. Analysis of the structure (Fig. 8A and B) using the DALI server (40) revealed that the cholesterol oxidase CYP142 from *Mycobacterium tuberculosis* 2XKR (41) was the closest structure to A24, with an rmsd of 1.9 Å over 395 C-alpha atoms, with few major differences between secondary elements making up the

structure(s). A major difference in the active site of CYP1232A24 compared to either PikC or 2XKR was the presence of a glutamate residue E240 (Fig. 8C) that replaced a threonine residue in positions 247 in PikC and 234 in 2XKR, respectively, which are thought to have a role in the scission of the dioxygen bond in the P450 catalytic cycle (41). Whilst other residues, such as proline, in CYP134A1 (42) and alanine in P450EryF (43) and P450XplA (44) have been observed at this position, glutamate is rarely observed. An analysis of a 3DM P450 superfamily database (https://www.bio-prodict.com, (45)) comprising of over 39,000 sequences suggests that only 0.2% of P450 sequences have a glutamate at this position. As a substrate of CYP1232A24, 3,4-DMPA was modelled into the active site using AutoDock VINA implemented in YASARA (46). The result exhibiting the lowest binding energy and thus strongest binding is shown in Fig. 8C where the *meta* methoxy group of 3,4-DMPA points towards the heme iron. In this orientation, the charged carboxylate of 3,4-DMPA interacts with the basic amino acid arginine (Arg82) and the backbone carbonyl of a methionine (Met285). The benzene ring of the substrate is further stabilized inside the predominantly hydrophobic pocket *via* van der Waals and hydrophobic interactions, such as the stabilizing aromatic hydrophobic phenylalanine (Phe386). This interplay leads to the coordination of the *meta* methoxy group above the heme, while there is still enough space inside the active pocket to enable the oxyfunctionalization of more bulky substrates such as 4-methoxycinnamic acid or naproxen (Fig. 8D).

Generation of efficient whole-cell biocatalysts

Due to the cofactor dependency of P450s, efficient whole-cell biocatalysts are obligatory for an application in industrial biocatalysis. Therefore, compatible dual-vector systems (pCola and pETDuet) were chosen for CYP1232F1, which permit simultaneous expression of up to four proteins under the control of a strong T7 promoter. Since an excess of flavodoxin or ferredoxin is crucial for high activities, these were cloned onto both plasmids. Furthermore, the pBAD33-compatible plasmid pBAD18 was selected for the co-expression of the redox partners for the whole-cell catalysis with CYP1232A24 due to its good expression in the pBAD33 vector and at the same time very low expression in the T7 promoter system pET-28a(+). The plasmids were constructed by Gibson Assembly®, and recombinant strains transformed with these plasmids were tested *in vivo* for 24 h using 0.1 g_{cww} ml^{-1} resting cells and

10 mM 3,4-DMPA or homovanillic acid. In case of the T7-based dual vectors, ~ 50% of the substrate 3,4-DMPA was selectively converted by CYP1232F1, FeRed_1 and FldX, corresponding to 0.93 ± 0.01 g l^{-1} of the product homovanillic acid (Table 3). In contrast, with CamA and CamB, a low *in vivo* activity was observed. Investigating whether this is caused by the actual activity of the P450 or by the redox partners themselves, cells from the same expression experiment were disrupted and the cell lysates subsequently analyzed by SDS-PAGE and CO-difference spectra (Table S11, Fig. S7). It turned out that the redox proteins were well expressed, but the CYP1232F1 was nearly completely in a nonfunctional state, characterized by a strong maximum at 420 nm in the CO-difference spectrum. By contrast, CYP1232A24 on pBAD33 was co-expressed with the compatible pBAD18 plasmid bearing FeRed_1 and FldX. The resulting whole-cell biocatalyst demethylated > 99% of 10 mM homovanillic acid, which corresponds to a product titer of 1.77 ± 0.04 g l^{-1} 3,4-dihydroxyphenylacetic acid.

Discussion

The identification of interesting oxygenases and possible clusters in the papaverine degrading *Arthrobacter* sp. provides insight into the function of oxygenases within the organism, putatively extending the available spectrum of efficient P450 catalysts for potential industrial applications. However, the identification of functional redox partners and suitable substrates is often a major challenge in exploiting the diverse, but complex, P450 enzymes from nature. In this study, proteomic and genomic analysis facilitated the elucidation of the physiological function of two P450s from *Arthrobacter* sp.

CYP1232A24 and F1 were detected in the proteomic analysis of *Arthrobacter* sp. cultures with papaverine as sole carbon source, implying their involvement in metabolism. The papaverine degradation pathway proposed by Lingens, Haase-Aschoff and Hauer (1979 and 1982) proceeds *via* the metabolite 3,4-dimethoxyphenylacetic acid, which is further processed by twofold demethylation (6, 9). The participation of cytochrome P450 monooxygenases at this step of the metabolic pathway was conceivable and has been finally confirmed by this study. While CYP1232F1 also accepted electrons from the non-physiological redox partners CamA and CamB, the physiological partners FeRed_1 and FldX could efficiently reconstitute the activity of both clustered P450s CYP1232A24 and F1. FldX is a

putative flavodoxin, which has high similarities to the FMN components of the nitrogen monoxide synthase reductases. In addition to the bifunctional reductases BMR from P450 BM3 and eukaryotic CPR, these belong to the FAD-FMN protein family (47). FldX further shows high amino acid sequence identity of 40% to known flavodoxins such as the cindoxin from *Citrobacter braakii*. Regarding the FAD-containing NADPH ferredoxin reductase FeRed_1, likewise high sequence identity of 35% relative to the putative cindoxin reductase from *C. braakii* was apparent. The reconstitution of the P450 activity by genetically clustered redox partners is rarely observed in microorganisms. In many cases, physiological redox partners are scattered over the entire genome and thus difficult to identify (39, 48, 49). Previous exceptions include the well-characterized P450cam, P450cin and P450terp which occur in clusters with their redox partners and catalyze the first step of degradation of camphor, cineole and α-terpineol, respectively (50–52). Here, P450cin is the only class III P450 system so far, which, in contrast to class I systems such as P450cam, transfers electrons over flavodoxin (cindoxin) instead of an iron-sulfur protein (ferredoxin) (53, 54). However, associated physiological cindoxin reductase has so far not been produced heterologously in active form enabling the characterization of the whole physiological system (55). Similarly, CYP1232 family members identified in this work can most likely classified into rare P450 class III, since they receive their electrons from the physiological putative flavodoxin FldX. Accordingly, CYP1232A24 and F1 are likely to represent heterologous expressed examples of physiological and functional class III P450 multicomponent systems consisting of FldX and the NADPH ferredoxin reductase FeRed_1. However, the sequence annotation of FldX as FMN-containing flavodoxin could not be experimentally confirmed yet and is, therefore, an interesting target for further investigations.

Exploring different carboxylic acids revealed a quite narrow substrate specificity profile for CYP1232F1. The demethylation activity in the *para* position was significantly reduced when the methoxy group in the *meta* position was substituted by a hydroxy group (Fig. 4). Substrates bearing a methoxy group in the *meta* position, such as 3-methoxyphenylacetic acid, were accepted, nevertheless showing a significant loss of activity. While benzoic acid and cinnamic acid derivatives were not oxyfunctionalized, CYP1232F1 demethylated eugenol and 3-chloro-4-methoxyaniline, which do not contain any carboxy groups. In contrast, CYP1232A24 represents a relatively versatile enzyme, which

was able to demethylate benzoic, phenylacetic and cinnamic acid derivatives as well as many other substituted aromatic compounds (Fig. 5). The relatively bulky molecule naproxen was, for example, demethylated to the human drug metabolite 6-*o*-desmethylnaproxen, while β-ionone could be hydroxylated to produce 4-hydroxy-β-ionone, a valuable precursor of flavors (56). Generally, substrates bearing a methoxy group in the *meta* position were preferred and showed higher activity compared to those without this group. These findings indicate a much more flexible and larger active pocket compared to CYP1232F1. In CYP1232A24, modelling suggests that the *meta* methoxy group of 3,4-DMPA is mainly coordinated above the heme by combined interactions of the substrate carboxylate with Arg82 as anchoring residue as well as hydrophobic interactions of the benzene ring in the active pocket. When comparing the active site residues of CYP1232A24 (Fig. 8C) with the corresponding residues in CYP1232F1, high similarity can be observed (Table 4) including Glu240, Arg82 and Phe386. The minor variations, e.g. Thr172 instead of Ala170 or Tyr286 instead of Val286, are therefore crucial for the determination of the regioselectivity of the enzymes that share 41% amino acid sequence identity in total (Fig. S8). These residues may also justify a larger active pocket of CYP1232A24 with considerable more space depicted by the surface display in Fig. 8D which enables the oxyfunctionalization of a broader panel of partially bulkier substrates.

Finally, the results of *in vitro* and spin-state experiments with CYP1232A24 and F1 ultimately led to two possible routes in the papaverine-metabolism, with one pathway apparently preferred over the other. Here, 3,4-DMPA is regioselectively demethylated in the *para* position to homovanillic acid by CYP1232F1. Through further demethylation in the *meta* position by CYP1232A24, 3,4-dihydroxyphenylacetic acid is produced for further degradation (Fig. 9). The alternative route could proceed without the participation of CYP1232F1 due to the versatile reaction spectrum of CYP1232A24. CYP1232A24 shows selectivity for demethylation in the *meta* position, nevertheless demethylation in the *para* or *meta* positions as well as a mix thereof is conceivable, since both resulting compounds were oxidized by CYP1232A24. Due to the catalytic properties of the enzymes and the detection of CYP1232A24 and F1 by proteomic analysis, the main proportion is presumably achieved over the route with both enzymes. This is consistent with the work of Hauer and co-workers (1982) in which homovanillic acid was detected as a metabolite in papaverine degrading *Arthrobacter* sp. (9).

The first step of this complex metabolic pathway is presumably catalyzed by an initial dihydroxylation of the heteroaromatic isoquinoline moiety of papaverine through a dioxygenase (6). In other microbial studies, different demethylated products of papaverine were isolated from biotransformations (57). However, such an activity towards papaverine could not be detected by CYP1232A24 and F1. The P450s were also not able to oxyfunctionalize the terpenes that *Arthrobacter* sp. utilizes as energy source. Therefore, the identity of other enzymes involved in the metabolism of sesquiterpenes like β-bisabolene and premnaspirodiene could not be resolved. Based on the proteomic analysis, further investigations will be carried out, which might reveal novel oxygenases for terpene oxyfunctionalization.

The complete physiological systems of CYP1232A24 and F1 achieved very high efficiencies *in vitro*. > 99% of the electrons originating from the cofactor NADPH were transferred into product formation. The preference of the reductase FeRed_1 for the cofactor NADPH was significantly higher than that of NADH (Table S10), which can be found in many P450 reductases (58). Overall, the enzymes investigated achieved high catalytic efficiencies (Table 3). In comparison to the heterologous redox partners CamA and CamB, an approximately twofold higher specific activity and thus efficiency was measured with CYP1232A24 and the physiological system FeRed_1 and FldX. In fact, this was often found in the literature, as in the case of the exchange of CamB to the physiological ferredoxin Pux with CYP199A2 (59, 60). The kinetics and binding affinities achieved are generally lower compared to CYP199A2 and A4 from *R. palustris*, although partly also the physiological redox partners and substrates were investigated (29). Nevertheless, both *Arthrobacter* sp. P450s displayed high *in vitro* activities and demethylated > 99% of 2 mM substrate within 30 min. Interestingly, FeRed_1 could also transfer electrons to CamB that led to half of the conversion of CYP1232F1 when applying CamA and CamB (data not shown).

For the generation of whole-cell systems, the combination of the compatible pBAD33 and pBAD18 expression vectors proved to be highly effective under the control of the strictly regulated arabinose promoters. This system is known to efficiently express toxic proteins (61). The high product yields of 1.77 g l^{-1} (CYP1232A24) show that the P450 as well as the redox partners are functionally expressed in high titers (Table 3). This result is well in line with previously described *in vivo* carboxylic acid hydroxylase systems CYP199A2 and A4 (29, 62, 63). Furthermore, CYP1232A24 was able to

exceed the *in vivo* yields of the so far only class III system P450cin (1.0 g l^{-1} product after 3 d) within 24 h (64). In the case of the pETDuet and pCola system with CYP1232F1, it is possible to simultaneously express four proteins each under the control of its own strong T7 promoter. Using CYP101C1 and CYP101B1 from *N. aromaticivorans*, this expression system successfully generated efficient whole-cell biocatalysts (48, 65). However, analysis of CYP1232F1 biotransformations showed that the enzyme was only poorly produced and almost completely in non-functional form. In view of this, a strong increase using the pBAD system can be expected. The strict regulation of the expression in the pBAD system appears to be a decisive factor in the production of the cell-toxic P450s compared to the often leaky expression with T7-containing vectors (66, 67).

In summary, two novel P450s from the papaverine degrading *Arthrobacter* sp. have been expressed and their activities characterized. Investigation by genomic and proteomic analysis facilitated the reconstitution of the enzymes' activity with clustered physiological redox partners. Accordingly, substrate specificity profiles, coupling efficiencies and binding as well as kinetic constants were determined which prove the physiological function of both CYPs in the papaverine degradation by *Arthrobacter* sp. The structure of CYP1232A24 has revealed an unusual glutamate residue in the active site in place of the well-conserved threonine in P450s, and modelling has suggested a basis for the regiopreference in the demethylation activity of the enzyme. The discovery of two functional P450 systems which can be presumably classified into P450s of class III will enable further analysis of this rarely observed electron transfer system complementing P450 research. Moreover, the construction of efficient whole-cell biocatalysts paves the way to implement the *Arthrobacter* sp. P450s into synthetic applications taking advantage of the high regioselectivity of oxyfunctionalization. The final product 3,4-dihydroxyphenylacetic acid is also an intermediate in the metabolism of dopamine as well as quercetin and exhibits antiproliferative activities (68–70); thus, it can also serve as building block for drugs containing catechols and phenylacetic acid moieties, respectively. Recently, the spectrum of catalyzed reactions of the benzoic acid hydroxylase CYP199A4 could be enlarged including heteroatom oxidation (71). Further investigation of the substrate and reaction spectrum of CYP1232A24 in combination with the possibility of a rational design approach improving this enzyme's properties may further extend its synthetic potential.

Funding:

The research leading to these results has received funding from the European Union's Seventh Framework Programme for research, technological development and demonstration under grant agreements no 613849 (BIOOX), as well as fellowship to J.M.K. from the Landesgraduiertenförderung (LSFG) Baden-Württemberg.

Acknowledgments: We would like to thank Dr. Sara Hoffmann and Dr. Leonie Weinmann for providing pETDuet_CamA_CamB and pBAD18 (two promoters), respectively. We thank Dr. Ondrej Reznicek, Berit Würtz and Dr. Jens Pfannstiel for helpful advice concerning cultivation of *Arthrobacter* sp. and the proteomic analysis. We thank Dr Johan P. Turkenburg and Mr Sam Hart for assistance with X-ray data collection, and the Diamond Light Source for access to beamline I04-1 under proposal number mx-9948.

Conflict of interest: The authors declare that they have no conflicts of interest with the contents of this article.

References

1. Busse, H.-J., and Wieser, M. (2014) The Genus *Arthrobacter*. in *The Prokaryotes - Actinobacteria*, 4th Ed. (Rosenberg, E., DeLong, E. F., Lor, S., Stackebrandt, E., and Thompson, F. eds), pp. 105–132, Springer Berlin Heidelberg, Heidelberg, 10.1007/0-387-30743-5

2. Robinson, J. B., Salonius, P. O., and Chase, F. E. (1965) A note on the differential response of *arthrobacter* spp. and *pseudomonas* spp. to drying in soil. *Can. J. Microbiol.* **11**, 746–748

3. Boylen, C. W. (1973) Survival of *Arthrobacter crystallopoietes* during prolonged periods of extreme desiccation. *J. Bacteriol.* **113**, 33–37

4. Labeda, D. P., Liu, K. C., and Casida, L. E. (1976) Colonization of soil by *Arthrobacter* and *Pseudomonas* under varying conditions of water and nutrient availability as studied by plate counts and transmission electron microscopy. *Appl. Environ. Microbiol.* **31**, 551–561

5. Marshall, S. J., and White, G. F. (2001) Complete denitration of nitroglycerin by bacteria isolated from a washwater soakaway. *Appl. Environ. Microbiol.* **67**, 2622–2626

6. Haase-Aschoff, K., and Lingens, F. (1979) Mikrobieller Abbau von Papaverin. *Hoppe. Seylers. Z. Physiol. Chem.* **360**, 621–632

7. Strong, L. C., Rosendahl, C., Johnson, G., Sadowsky, M. J., and Wackett, L. P. (2002) *Arthrobacter aurescens* TC1 metabolizes diverse s-triazine ring compounds. *Appl. Environ. Microbiol.* **68**, 5973–5980

8. Gil, M., Haïdour, A., and Ramos, J. L. (2000) Degradation of o-methoxybenzoate by a two-member consortium made up of a gram-positive *Arthrobacter* strain and a gram-negative *Pantotea* strain. *Biodegradation*. **11**, 49–53

9. Hauer, B., Haase-Aschoff, K., and Lingens, F. (1982) Papaverine degradation with papaverine mutants of a *Nocardia* sp. *Hoppe. Seylers. Z. Physiol. Chem.* **363**, 499–506

10. Eaton, R. W. (2001) Plasmid-encoded phthalate catabolic pathway in *Arthrobacter keyseri* 12B. *J. Bacteriol.* **183**, 3689–3703

11. Pieper, D. H. (2005) Aerobic degradation of polychlorinated biphenyls. *Appl. Microbiol. Biotechnol.* **67**, 170–191

12. Deng, Y., Mao, Y., Li, B., Yang, C., and Zhang, T. (2016) Aerobic degradation of sulfadiazine by *Arthrobacter* spp.: Kinetics, pathways, and genomic characterization. *Environ. Sci. Technol.* **50**, 9566–9575

13. Bhosle, S., Kaliwal, S. M., Paknikar, S. K., and Mavinkurve, S. (1993) Molecular rearrangement of longifolene by molecular rearrangement of longifolene by *Arthrobacter ilicis* T2. *Appl. Environ. Microbiol.* **59**, 2–5

14. Munro, A. W., Girvan, H. M., and McLean, K. J. (2007) Cytochrome P450-redox partner fusion enzymes. *Biochim. Biophys. Acta - Gen. Subj.* **1770**, 345–359

15. Hannemann, F., Bichet, A., Ewen, K. M., and Bernhardt, R. (2007) Cytochrome P450 systems-biological variations of electron transport chains. *Biochim. Biophys. Acta - Gen. Subj.* **1770**, 330–344

16. Urlacher, V. B., and Girhard, M. (2012) Cytochrome P450 monooxygenases: an update on perspectives for synthetic application. *Trends Biotechnol.* **30**, 26–36

17. Klenk, J. M., Nebel, B. A., Porter, J. L., Kulig, J. K., Hussain, S. A., Richter, S. M., Tavanti, M., Turner, N. J., Hayes, M. A., Hauer, B., and Flitsch, S. L. (2017) The self-sufficient P450 RhF expressed in a whole cell system selectively catalyses the 5-hydroxylation of diclofenac. *Biotechnol. J.* **12**, 1–8

18. Bernhardt, R. (2006) Cytochromes P450 as versatile biocatalysts. *J. Biotechnol.* **124**, 128–145

19. Bleif, S., Hannemann, F., Lisurek, M., von Kries, J. P., Zapp, J., Dietzen, M., Antes, I., and Bernhardt, R. (2011) Identification of CYP106A2 as a regioselective allylic bacterial diterpene hydroxylase. *Chembiochem*. **12**, 576–582

20. Klenk, J. M., Dubiel, P., Sharma, M., Grogan, G., and Hauer, B. (2018) Characterization and structure-guided engineering of the novel versatile terpene monooxygenase CYP109Q5 from

Chondromyces apiculatus DSM436. *Microb. Biotechnol.* **in press**, DOI:10.1111/1751-7915.13354

21. Bell, S. G., and Wong, L.-L. (2007) P450 enzymes from the bacterium *Novosphingobium aromaticivorans*. *Biochem. Biophys. Res. Commun.* **360**, 666–672

22. Bell, S. G., Hoskins, N., Xu, F., Caprotti, D., Rao, Z., and Wong, L. L. (2006) Cytochrome P450 enzymes from the metabolically diverse bacterium *Rhodopseudomonas palustris*. *Biochem. Biophys. Res. Commun.* **342**, 191–196

23. Khatri, Y., Hannemann, F., Ewen, K. M., Pistorius, D., Perlova, O., Kagawa, N., Brachmann, A. O., Müller, R., and Bernhardt, R. (2010) The CYPome of *sorangium cellulosum* so ce56 and identification of CYP109D1 as a new fatty acid hydroxylase. *Chem. Biol.* **17**, 1295–1305

24. Reznicek, O., Facey, S. J., and Hauer, B. (2015) Draft genome sequence of a papaverine-degrading, gram-positive *Arthrobacter* sp., isolated from soil near Hohenheim, Germany. *Genome Announc*. **3**, 1999–2000

25. Cohen-Bazire, G., Sistrom, W. R., and Stanier, R. Y. (1957) Kinetic studies of pigment synthesis by non-sulfur purple bacteria. *J. Cell. Comp. Physiol.* **49**, 25–68

26. Voolstra, O., Beck, K., Oberegelsbacher, C., Pfannstiel, J., and Huber, A. (2010) Light-dependent phosphorylation of the *Drosophila* transient receptor potential ion channel. *J. Biol. Chem.* **285**, 14275–14284

27. Vizcaíno, J. A., Csordas, A., Del-Toro, N., Dianes, J. A., Griss, J., Lavidas, I., Mayer, G., Perez-Riverol, Y., Reisinger, F., Ternent, T., Xu, Q. W., Wang, R., and Hermjakob, H. (2016) 2016 update of the PRIDE database and its related tools. *Nucleic Acids Res.* **44**, D447–D456

28. Omura, T., and Sato, R. (1964) The carbon monoxide-binding pigment of liver microsomes. *J. Biol. Chem.* **239**, 2370–2378

29. Bell, S. G., Tan, A. B. H., Johnson, E. O. D., and Wong, L.-L. (2010) Selective oxidative demethylation of veratric acid to vanillic acid by CYP199A4 from *Rhodopseudomonas palustris*

HaA2. *Mol. BioSyst.* **6**, 206–214

30. Purdy, M. M., Koo, L. S., Ortiz de Montellano, P. R., and Klinman, J. P. (2004) Steady-state kinetic investigation of cytochrome P450cam: interaction with redox partners and reaction with molecular oxygen. *Biochemistry*. **43**, 271–281

31. Atkin, K. E., Reiss, R., Turner, N. J., Brzozowski, A. M., and Grogan, G. (2008) Cloning, expression, purification, crystallization and preliminary X-ray diffraction analysis of variants of monoamine oxidase from *Aspergillus niger*. *Acta Crystallogr. Sect. F Struct. Biol. Cryst. Commun.* **64**, 182–185

32. Kabsch, W. (2010) Xds. *Acta Crystallogr. Sect. D Biol. Crystallogr.* **66**, 125–132

33. Evans, P. (2006) Scaling and assessment of data quality. *Acta Crystallogr. Sect. D Biol. Crystallogr.* **62**, 72–82

34. Winter, G. (2010) Xia2: An expert system for macromolecular crystallography data reduction. *J. Appl. Crystallogr.* **43**, 186–190

35. Vagin, A. A., and Teplyakov, A. (1997) Molrep: An automated program for molecular replacement. *J. Appl. Crystallogr.* **30**, 1022–1025

36. Li, S., Ouellet, H., Sherman, D. H., and Podust, L. M. (2009) Analysis of transient and catalytic desosamine-binding pockets in cytochrome P-450 PikC from *Streptomyces venezuelae*. *J. Biol. Chem.* **284**, 5723–5730

37. Emsley, P., and Cowtan, K. (2004) Coot: model-building tools for molecular graphics. *Acta Crystallogr. D. Biol. Crystallogr.* **60**, 2126–2132

38. Murshudov, G. N., Vagin, A. A., and Dodson, E. J. (1997) Refinement of macromolecular structures by the maximum-likelihood method. *Acta Crystallogr. Sect. D Biol. Crystallogr.* **53**, 240–255

39. McLean, K. J., Luciakova, D., Belcher, J., Tee, K. L., and Munro, A. W. (2015) Biological diversity of cytochrome P450 redox partner systems. in *Monooxygenase, Peroxidase and*

Peroxygenase Properties and Mechanisms of Cytochrome P450 (Hrycay, E. G., and Bandiera, S. M. eds), pp. 299–317, Springer International Publishing, Cham, 10.1007/978-3-319-16009-2_11

40. Holm, L., and Laakso, L. M. (2016) Dali server update. *Nucleic Acids Res.* **44**, W351–W355

41. Driscoll, M. D., McLean, K. J., Levy, C., Mast, N., Pikuleva, I. A., Lafite, P., Rigby, S. E. J., Leys, D., and Munro, A. W. (2010) Structural and biochemical characterization of *Mycobacterium tuberculosis* CYP142: Evidence for multiple cholesterol 27-hydroxylase activities in a human pathogen. *J. Biol. Chem.* **285**, 38270–38282

42. Cryle, M. J., Bell, S. G., and Schlichting, I. (2010) Structural and biochemical characterization of the cytochrome P450 CypX (CYP134A1) from *bacillus subtilis*: A cyclo-l-leucyl-l-leucyl dipeptide oxidase. *Biochemistry*. **49**, 7282–7296

43. Nagano, S., Cupp-Vickery, J. R., and Poulos, T. L. (2005) Crystal structures of the ferrous dioxygen complex of wild-type cytochrome P450eryF and its mutants, A245S and A245T: Investigation of the proton transfer system in P450eryF. *J. Biol. Chem.* **280**, 22102–22107

44. Sabbadin, F., Jackson, R., Haider, K., Tampi, G., Turkenburg, J. P., Hart, S., Bruce, N. C., and Grogan, G. (2009) The 1.5-Å structure of XplA-heme, an unusual cytochrome P450 heme domain that catalyzes reductive biotransformation of royal demolition explosive. *J. Biol. Chem.* **284**, 28467–28475

45. Kuipers, R. K., Joosten, H. J., Van Berkel, W. J. H., Leferink, N. G. H., Rooijen, E., Ittmann, E., Van Zimmeren, F., Jochens, H., Bornscheuer, U., Vriend, G., Martins Dos Santos, V. A. P., and Schaap, P. J. (2010) 3DM: Systematic analysis of heterogeneous superfamily data to discover protein functionalities. *Proteins Struct. Funct. Bioinforma.* **78**, 2101–2113

46. Trott, O., and Olson, A. J. (2010) AutoDock Vina: improving the speed and accuracy of docking with a new scoring function, efficient optimization and multithreading. *J. Comput. Chem.* **31**, 455–461

47. Iyanagi, T. (2005) Structure and function of NADPH-cytochrome P450 reductase and nitric

oxide synthase reductase domain. *Biochem. Biophys. Res. Commun.* **338**, 520–528

48. Bell, S. G., Dale, A., Rees, N. H., and Wong, L.-L. (2010) A cytochrome P450 class I electron transfer system from *Novosphingobium aromaticivorans*. *Appl. Microbiol. Biotechnol.* **86**, 163–175

49. Ewen, K. M., Hannemann, F., Khatri, Y., Perlova, O., Kappl, R., Krug, D., Hütterman, J., Müller, R., and Bernhardt, R. (2009) Genome mining in *Sorangium cellulosum* So ce56: Indentification characterization of the homologous electron transfer proteins of a Myxobacterial cytochrome P450. *J. Biol. Chem.* **284**, 28590–28598

50. Hawkes, D. B., Adams, G. W., Burlingame, A. L., Ortiz De Montellano, P. R., and De Voss, J. J. (2002) Cytochrome P450cin (CYP176A), isolation, expression, and characterization. *J. Biol. Chem.* **277**, 27725–27732

51. Peterson, J. A. (1971) Camphor binding by *Pseudomonas putida* cytochrome P-450. *Arch Biochem Biophys*. **144**, 678–693

52. Peterson, J. A., Lu, J., Geisselsoder, J., Graham-lorence, S., Carmona, C., Witney, F., and Lorence, M. C. (1992) Cytochrome P-450terp. *J. Biol. Chem.* **267**, 14193–14203

53. Kimmich, N., Das, A., Sevrioukova, I., Meharenna, Y., Sligar, S. G., and Poulos, T. L. (2007) Electron transfer between cytochrome P450cin and its FMN-containing redox partner, Cindoxin. *J. Biol. Chem.* **282**, 27006–27011

54. Stok, J. E., Yamada, S., Farlow, A. J., Slessor, K. E., and De Voss, J. J. (2013) Cytochrome P450cin (CYP176A1) D241N: Investigating the role of the conserved acid in the active site of cytochrome P450s. *Biochim. Biophys. Acta - Proteins Proteomics*. **1834**, 688–696

55. Hawkes, D. B., Slessor, K. E., Bernhardt, P. V, and De Voss, J. J. (2010) Cloning, expression and purification of Cindoxin, an unusual Fmn-containing cytochrome P450 redox partner. *ChemBioChem*. **11**, 1107–1114

56. Serra, S. (2015) Recent advances in the synthesis of carotenoid-derived flavours and fragrances.

Molecules. **20**, 12817–12840

57. Rosazza, J. P., Kammer, M., Youel, L., Smith, R. V., Erhardt, P. W., Truong, D. H., and Leslie, S. W. (1977) Microbial models of mammalian metabolism *O*-demethylations of papaverine. *Xenobiotica*. **7**, 133–143

58. Lundemo, M. T., and Woodley, J. M. (2015) Guidelines for development and implementation of biocatalytic P450 processes. *Appl. Microbiol. Biotechnol.* **99**, 2465–2483

59. Bell, S. G., Xu, F., Forward, I., Bartlam, M., Rao, Z., and Wong, L. L. (2008) Crystal Structure of CYP199A2, a *para*-substituted benzoic acid oxidizing cytochrome P450 from *Rhodopseudomonas palustris*. *J. Mol. Biol.* **383**, 561–574

60. Furuya, T., and Kino, K. (2010) Regioselective oxidation of indole- and quinolinecarboxylic acids by cytochrome P450 CYP199A2. *Appl. Microbiol. Biotechnol.* **85**, 1861–1868

61. Saïda, F., Uzan, M., Odaert, B., and Bontems, F. (2006) Expression of highly toxic genes in *E. coli*: special strategies and genetic tools. *Curr. Protein Pept. Sci.* **7**, 47–56

62. Furuya, T., Arai, Y., and Kino, K. (2012) Biotechnological production of caffeic acid by bacterial cytochrome P450 CYP199A2. *Appl. Environ. Microbiol.* **78**, 6087–6094

63. Furuya, T., Shitashima, Y., and Kino, K. (2015) Alteration of the substrate specificity of cytochrome P450 CYP199A2 by site-directed mutagenesis. *J. Biosci. Bioeng.* **119**, 47–51

64. Slessor, K. E., Hawkes, D. B., Farlow, A., Pearson, A. G., Stok, J. E., and Voss, J. J. De (2012) An *in vivo* cytochrome P450 cin (CYP176A1) catalytic system for metabolite production. *J. Mol. Catal. B. Enzym.* **79**, 15–20

65. Hall, E. A., and Bell, S. G. (2015) The efficient and selective biocatalytic oxidation of norisoprenoid and aromatic substrates by CYP101B1 from *Novosphingobium aromaticivorans* DSM12444. *RSC Adv.* **5**, 5762–5773

66. Rosano, G. L., and Ceccarelli, E. A. (2014) Recombinant protein expression in *Escherichia coli*: Advances and challenges. *Front. Microbiol.* **5**, 1–17

67. Guzman, L.-M., Belin, D., Carson, M. J., and Beckwith, J. (1995) Tight regulation, modulation, and high-level expression by vectors containing the arabinose PBAD promoter. *J. Bacteriol.* **177**, 4121–4130

68. Tralma, K., Gotteland, M., and Carrasco-pozo, C. (2017) 3,4-Dihydroxyphenylacetic acid , a microbial metabolite of quercetin, protects intestinal and pancreatic beta cell lines from the cytotoxicity induced by rotenone. *SL Nutr. Metab.* **1**, 8–12

69. Meiser, J., Weindl, D., and Hiller, K. (2013) Complexity of dopamine metabolism. *Cell Commun. Signal.* **11**, 1–18

70. Tang, Y., Nakashima, S., Saiki, S., Myoi, Y., Abe, N., Kuwazuru, S., Zhu, B., Ashida, H., Murata, Y., and Nakamura, Y. (2016) 3,4-Dihydroxyphenylacetic acid is a predominant biologically-active catabolite of quercetin glycosides. *Food Res. Int.* **89**, 716–723

71. Coleman, T., Wong, S. H., Podgorski, M. N., Bruning, J. B., De Voss, J. J., and Bell, S. G. (2018) The cytochrome P450 CYP199A4 from *Rhodopseudomonas palustris* catalyses heteroatom dealkylations, sulfoxidation and amide and cyclic hemiacetal formation. *ACS Catal.* **8**, 5915–5927

Tables

Table 1. Data collection and refinement statistics for CYP1232A24. Numbers in brackets refer to data for highest resolution shells.

	CYP1232A24
Beamline	Diamond I04-1
Wavelength (Å)	0.91587
Resolution (Å)	52.92-1.70 (1.74-1.70)
Space Group	$P2_1$
Unit cell (Å)	a = 39.39; b = 100.83; c = 53.42 α = γ = 90.00°; β = 97.85
No. of molecules in the asymmetric unit	1
Unique reflections	44239 (3185)
Completeness (%)	97.6 (95.8)
R_{merge} (%)	0.19 (0.69)
$R_{p.i.m.}$	0.16 (0.61)
Multiplicity	4.1 (3.4)
$\langle I/\sigma(I)\rangle$	4.5 (1.2)
Overall *B* factor from Wilson plot (Å^2)	18
$CC_{1/2}$	0.94 (0.55)
R_{cryst}/ R_{free} (%)	20.8/22.9
r.m.s.d 1-2 bonds (Å)	0.015
r.m.s.d 1-3 angles (°)	1.55
Avg. main chain B (Å^2)	25
Avg. side chain B (Å^2)	28
Avg. water B (Å^2)	33

Table 2. Proteomic analysis of *Arthrobacter* sp. The cells were cultivated with different carbon sources. The debris fractions are similar to the lysate fractions and are therefore not shown for clarity. The number stands for the number of clearly attributable peptide fragments to a protein. A higher number implies a higher probability that the protein is present in the sample. Other relevant proteins that could not be detected in proteome analysis (-) but can be assigned to potential clusters are also presented.

	Identified proteins (In total 76)	Molecular weight [kDa]	Carbon source	
			Glucose	Papaverine
Cluster 1	**CYP1232A24**	46	-	**7**
	CYP1232F1	44	-	**6**
	Ferredoxin reductase ≙ **FeRed_1**	43	-	**4**
	Flavodoxin ≙ **FldX**	20	-	-
	Flavin reductase ≙ **FlavRed**	22	-	-

Table 3. Biochemical characterization of the *Arthrobacter* sp. P450s *in vitro* and *in vivo*. CYP1232A24 and F1 were investigated with homovanillic acid and 3,4-dimethoxyphenylacetic acid, respectively.

						Product formation	
P450	**Redox partner**	**Coupling efficiency** [a] [%]	K_m [µM]	k_{cat} [min^{-1}]	k_{cat} K_m^{-1} [min^{-1} M^{-1}]	***In vitro*** [b] [%]	***In vivo*** [c] [g l^{-1}]
CYP1232A24	FeRed_1/FldX	**87.0** ± 0.8	**6.69** ± 0.27	**5.23** ± 0.28	**$7.82*10^5$**	**99.8** ± 1.0	**1.77** ± 0.04
CYP1232F1	FeRed_1/FldX	**99.5** ± 0.5	**5.16** ± 0.17	**5.4** ± 0.03	**$1.05*10^6$**	**99.9** ± 2.9	**0.93** ± 0.01
	CamA/B	**83.7** ± 1.0	**5.18** ± 0.20	**2.28** ± 0.04	**$4.40*10^5$**	**88.1** ± 2.8	**0.06** ± 0.01

a) The coupling efficiency represents the efficiency with which the cofactor NAD(P)H is used to form the product.

b) For the determination of *in vitro* product formation, 2 µM P450, 2 mM substrate and the G6PDH cofactor regeneration system were used and the reaction was stopped after 30 min by addition of HCl.

c) The analytical biotransformations were carried out in 1 ml at a cell concentration of 0.1 g_{cww} ml^{-1} for 24 h using 10 mM substrate. The reactions with CYP1232A24 was carried out in the pBAD33/pBAD18 system and the reactions with CYP1232F1 in the pETDuet/pCola system.

Table 4. Comparison of active site residues in CYP1232A24 and F1. The corresponding amino acids of CYP1232F1 in the 3D-space were identified by a P450 3DM database and blast search. CYP1232A24 and F1 have 41% amino acid identity over the whole structure. Differences between both enzymes are highlighted in red. The 3D numbering scheme represents the structurally conserved regions (core) in a (P450) superfamily and stands for an amino acid located in different proteins of the superfamily at the same position in three-dimensional space. - no 3DM number assigned.

3DM number	-	52	57	58	139	140	143	212
CYP1232A24	Met72	Met76	Leu81	Arg82	Leu166	Ile167	Ala170	Met232
CYP1232F1	Met74	Met78	Val83	Arg84	Leu168	Val169	Thr172	Leu232

3DM number	215	219	281	282	283	284	377	378
CYP1232A24	Gly235	Glu240	Ile283	Met285	Val286	Pro287	Val385	Phe386
CYP1232F1	Ala235	Glu240	Val283	Met285	Tyr286	Pro287	Ile385	Phe386

Figure legends

Figure 1. Postulated metabolic pathway of papaverine in *Arthrobacter* sp. (adapted from (6)). *Arthrobacter* sp. (formerly known as *Nocardia* sp.) is able to grow on the opium alkaloid papaverine as sole carbon and nitrogen source. A section of the postulated pathway is shown focusing on reactions which might be catalyzed by oxygenases. In the first step, papaverine is dihydroxylated at the heteroaromatic isoquinolin moiety (**M1**). Metabolite **M2** is presumably formed *via* rearomatization, dehydration, hydrolization and reductive desamination. The cleavage of **M2** to **M3a** and **M3b** is thought to be catalyzed by monooxygenases. 3,4-Dimethoxyphenylacetic acid (**M3a**) is further processed *via* demethylation steps over **M4** and **M5**. Finally, **M6** is formed by an extradiol-cleaving 3,4-dihydroxyphenylacetate 2,3-dioxygenase. The metabolite **M3b** is presumably metabolized in similar fashion by the same enzymes. The enzymes of the metabolic pathway of papaverine are not known so far.

Figure 2. Potential cluster on the genome of *Arthrobacter* sp. The P450s identified by proteomic analysis with papaverine as the sole carbon source lie directly behind each other on the genome and are clustered with their potential redox partners in the near environment (FldX, FeRed_1 and FlavRed). The cluster is located on scaffold 2 (1.1 Mb), which is one of three scaffolds obtained by whole-genome shotgun sequencing of *Arthrobacter* sp.

Figure 3. Protein purification of the P450s from *Arthrobacter* sp. CYP1232A24 and F1 were partially purified through IEX. The eluates were separated on 15% SDS gels according to their molecular weight. Reduced CO-difference spectra of the partially purified enzymes were recorded indicating mostly functional P450 at a maximum of 446 nm and 450 nm, respectively.

Figure 4. Substrate specificity profile of CYP1232F1. Substrates are grouped by the product formation achieved with 2 µM CYP1232F1, 3 µM CamA and 30 µM CamB using 1 mM substrate and G6PDH cofactor regeneration system over 24 h. Only demethylated products were oberved. **1**: 3,4-Dimethoxyphenylacetic acid, **4**: Isohomovanillic acid, **5**: Eugenol, **6**: 3-Methoxyphenylacetic acid, **7**: 3-Chloro-4-methoxyanilin.

Figure 5. Substrate specificity profile of CYP1232A24. Substrates are grouped by the product formation achieved with 2 µM CYP1232F1, 3 µM FeRed_1 and 225 µM FldX solution using 1 mM substrate and G6PDH cofactor regeneration system over 24 h. Substrates without a methoxy group were hydroxylated. **1**: 3,4-Dimethoxyphenylacetic acid, **2**: Homovanillic acid, **4**: Isohomovanillic acid, **5**: Eugenol, **6**: 3-Methoxyphenylacetic acid, **7**: 3-Chloro-4-methoxyanilin, **8**: β-Ionone, **9**: Isovanillic acid, **10**: 4-Methoxybenzoic acid, **11**: 4-Methoxycinnamic acid, **12**: Naproxen, **13**: Lauric acid, **14**: Guajacole, **15**: 3-Hydroxy-4-methoxybenzaldehyde, **16**: 3-Methylanisol.

Figure 6. Spin state spectra of CYP1232F1 and CYP1232A24 from *Arthrobacter* sp. Substrate solutions of varying concentration (in DMSO) were added stepwise to a 3 µM P450 solution until substrate saturation (A_{max}) was reached. The high-spin shift ΔA was obtained by subtraction with the reference (P450 sample without substrate). Only selected spectra are shown. For the determination of the dissociation constant K_d, ΔA was plotted against the applied subtrate concentration and fitted in Excel using a hyperbolic curve. The measurements were performed in triplicates. **A**) CYP1232F1 with 3,4-dimethoxyphenylacetic acid (**1**); **B**) CYP1232A24 with homovanillic acid (**2**); **C**) CYP1232A24 with isohomovanillic acid (**4**).

Figure 7. Determination of kinetic constants of *Arthrobacter* sp. P450s. The following reactions were analyzed: **A**) CYP1232A24 with FeRed_1 and FldX catalyzed demethylation of homovanillic acid (**2**) to 3,4-dihydroxyphenylacetic acid (**3**); **B**) CYP1232F1 catalyzed demethylation of 3,4-dimethoxyphenylacetic acid (**1**) in *para* position to homovanillic acid (**2**) *via* the redox partners CamA and CamB or **C**) with FeRed_1 and FldX. The measurements were carried out in triplicates and the kinetic constants k_{cat} and K_m were determined by fitting with the Excel solver software.

Figure 8. Crystal structure and molecular docking of CYP1232A24. **A**) Monomer of CYP1232A24 with the heme in *orange*. Dotted purple lines represent gaps at positions 68-69 and 216-218; **B**) Surface display of CYP1232A24 showing the entrance to the active site; **C**) Docking of 3,4-dimethoxyphenylacetic acid as substrate (*green*) using the AutoDock Vina algorithm implemented in YASARA. The residues forming the active site are shown in *grey*; *red*: oxygens; *blue*: nitrogens; *yellow*: sulphurs; *magenta*: iron. **D**) Surface display of the active site viewing from the substrate tunnel onto the heme.

Figure 9. Participation of CYP1232A24 and F1 in the metabolic pathway of papaverine in *Arthrobacter* sp. The scheme was derived from Lingens, Haase-Aschoff, and Hauer (6, 9). Papaverine is processed to 3,4-dimethoxyphenylacetic acid (**1**) over several steps. ***Black* route**: Using the physiological electron transfer partners FeRed_1 and FldX the following degradation proceed through the sequential demethylation by CYP1232A24 and F1 *via* homovanillic acid (**2**) to 3,4-dihydroxyphenylacetic acid (**3**); ***Orange* route**: Both demethylation steps are catalyzed by CYP1232A24.

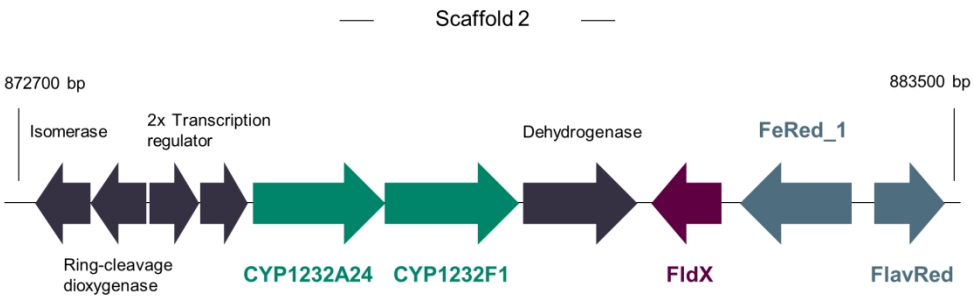

Figure 2. Potential cluster on the genome of *Arthrobacter* sp.

164x50mm (300 x 300 DPI)

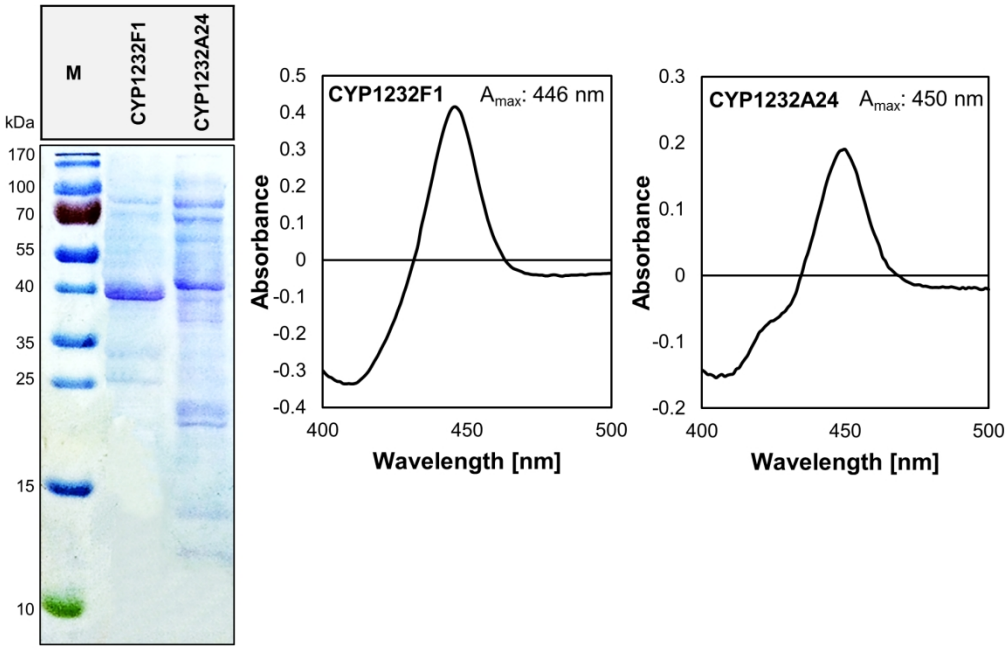

Figure 3. Protein purification of the P450s from *Arthrobacter* sp.

165x108mm (300 x 300 DPI)

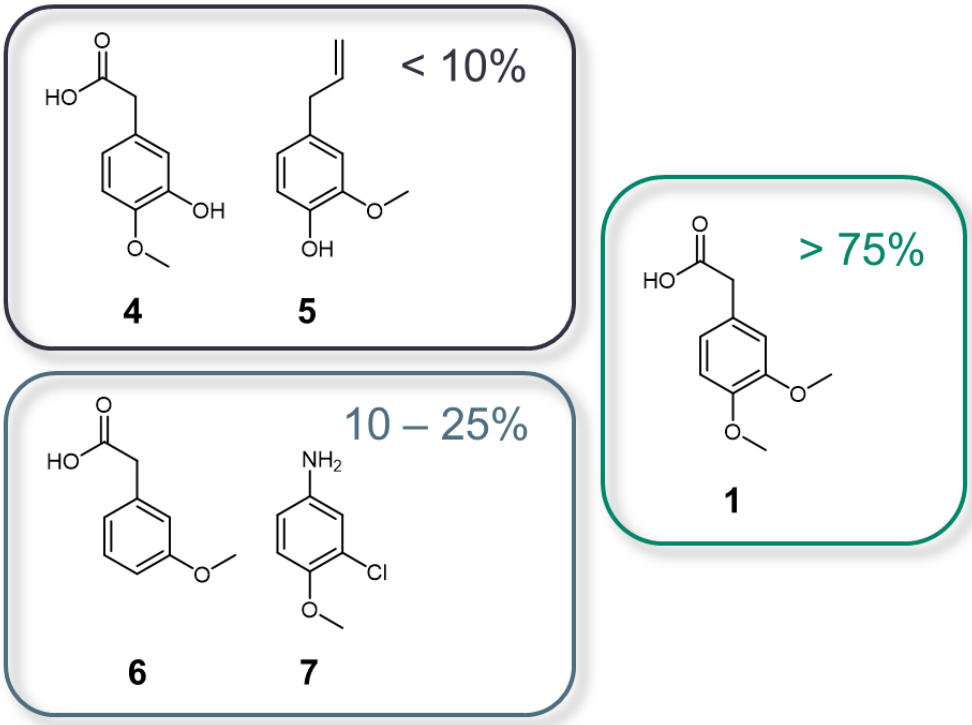

Figure 4. Substrate specificity profile of CYP1232F1.

78x59mm (300 x 300 DPI)

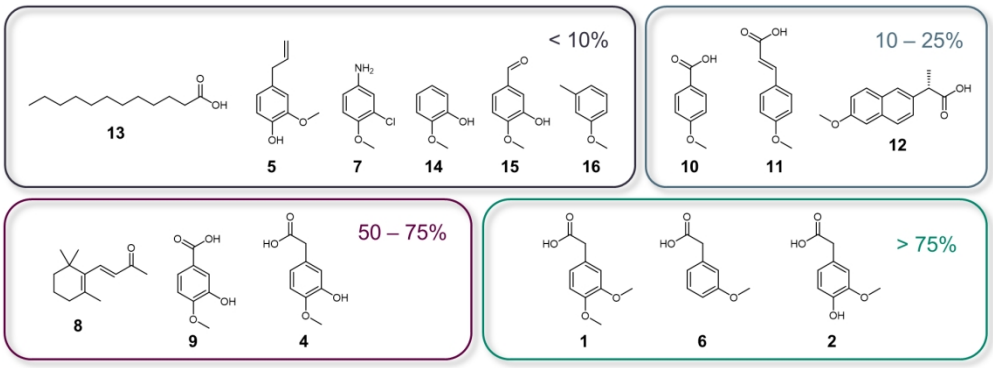

Figure 5. Substrate specificity profile of CYP1232A24.

165x60mm (300 x 300 DPI)

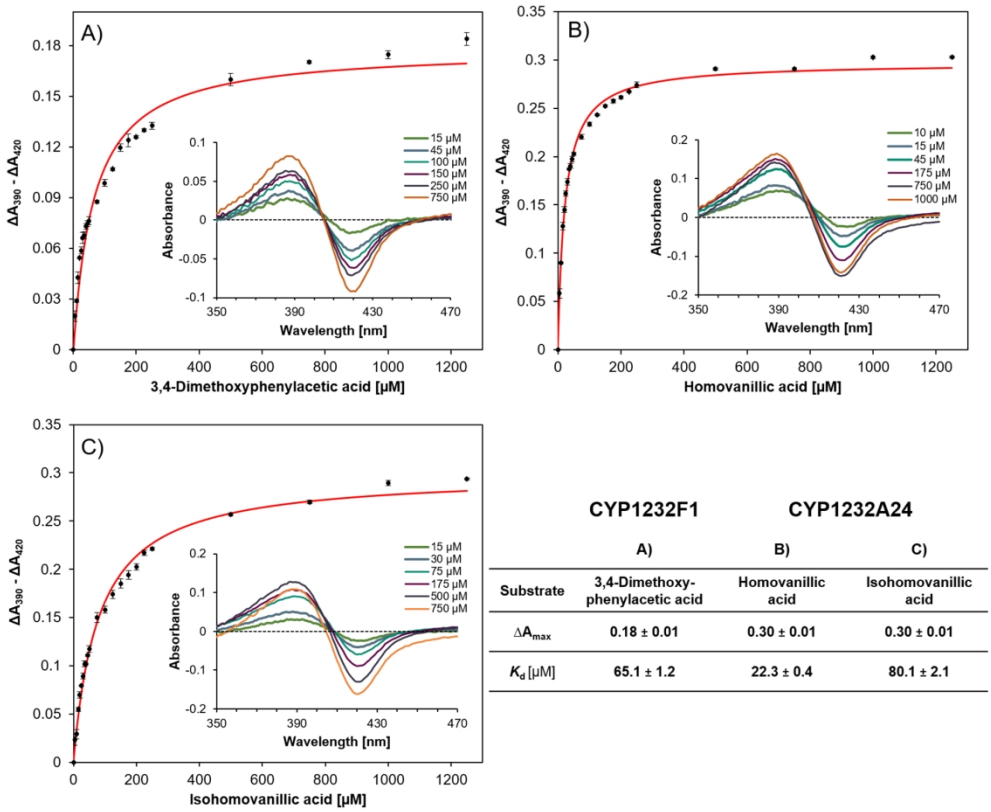

	CYP1232F1	CYP1232A24	
	A)	B)	C)
Substrate	3,4-Dimethoxy-phenylacetic acid	Homovanillic acid	Isohomovanillic acid
ΔA_{max}	0.18 ± 0.01	0.30 ± 0.01	0.30 ± 0.01
K_d [μM]	65.1 ± 1.2	22.3 ± 0.4	80.1 ± 2.1

Figure 6. Spin state spectra of CYP1232F1 and CYP1232A24 from *Arthrobacter* sp.

165x135mm (300 x 300 DPI)

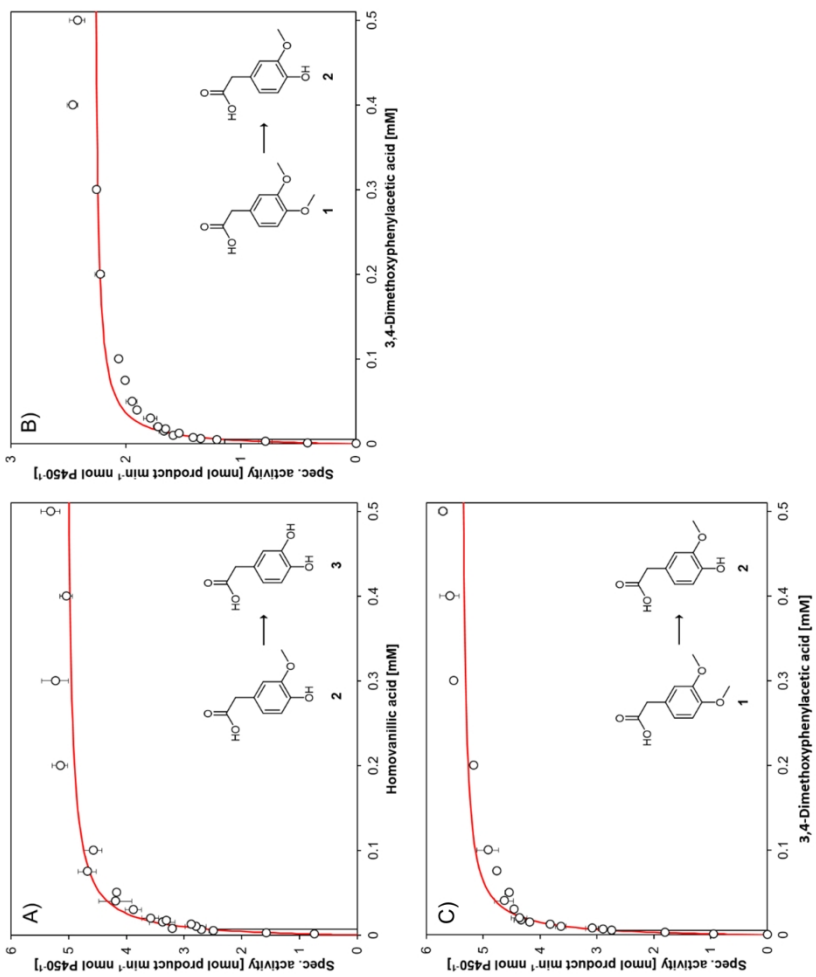

Figure 7. Determination of kinetic constants of *Arthrobacter* sp. P450s.

164x136mm (300 x 300 DPI)

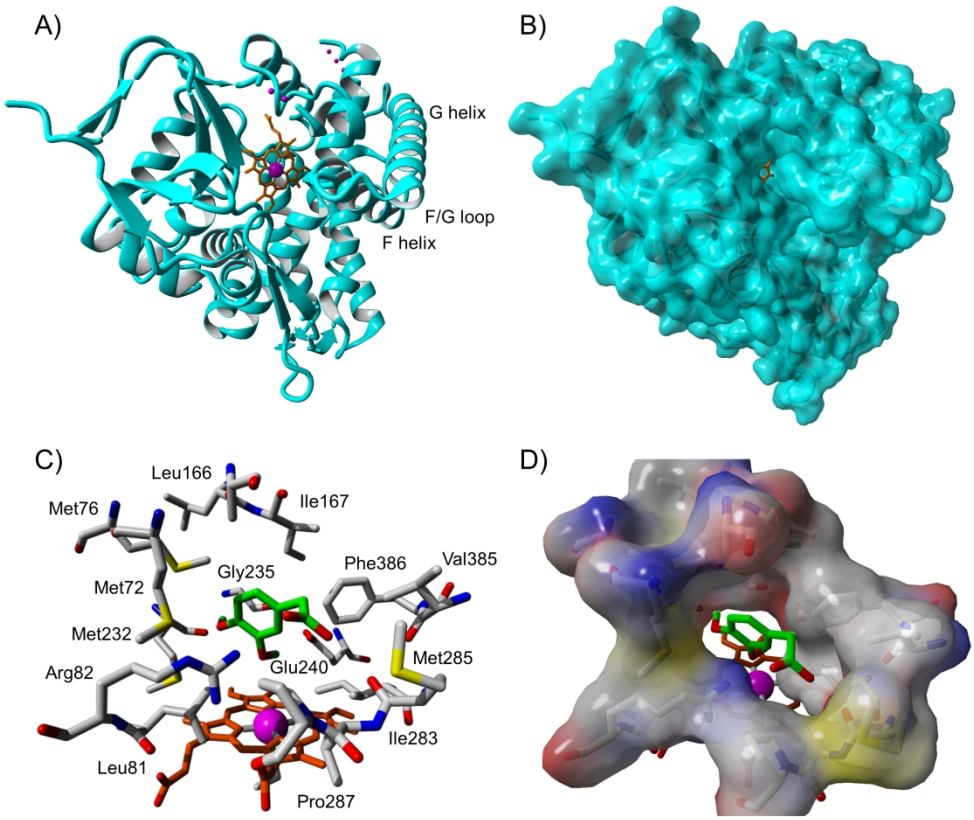

Figure 8. Crystal structure and molecular docking of CYP1232A24.

234x197mm (300 x 300 DPI)

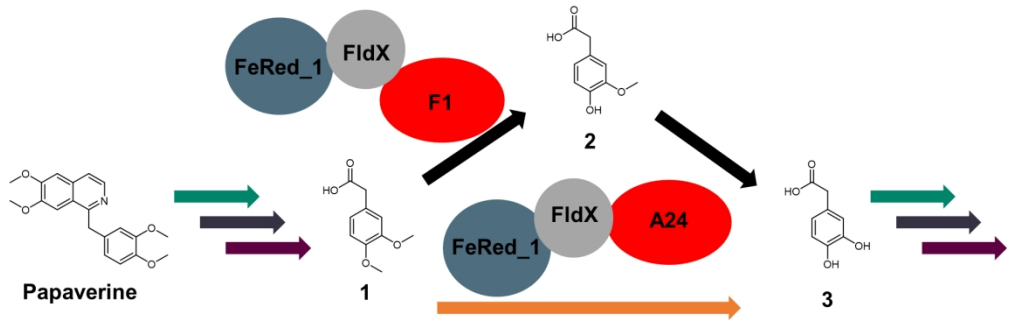

Figure 9. Participation of CYP1232A24 and F1 in the metabolic pathway of papaverine in *Arthrobacter* sp.

164x52mm (300 x 300 DPI)